Novel pyroptosis-related lncRNAs and ceRNAs predict osteosarcoma prognosis and indicate immune microenvironment signatures

Mingyi Yang, Haishi Zheng, Yani Su, Ke Xu, Qiling Yuan, Yongsong Cai, Yirixiati Aihaiti, Peng Xu[*]

Department of Joint Surgery, HongHui Hospital, Xi'an Jiaotong University, Xi'an, Shaanxi, 710054, China

ABSTRACT

Objective: To study pyroptosis-related biomarkers that are associated with the prognosis and immune microenvironment characteristics of osteosarcoma (OS). The goal is to establish a foundation for the prognosis and treatment of OS.

Methods: We retrieved transcriptome and clinical data from The Cancer Genome Atlas (TCGA) database for 88 OS patients. Using this data, we constructed a prognostic model to identify pyroptosis-related genes (PRGs) associated with OS prognosis. To further explore the biological function of these PRGs, we performed enrichment analysis. To identify pyroptosis-related long non-coding RNAs (PRLncs) associated with the prognosis of OS, we performed co-expression analysis. Subsequently, a risk prognostic model was constructed using these PRLncs to generate a risk score, termed as PRLncs-score, thereby obtaining PRLncs associated with the prognosis of OS. The accuracy of the prognostic model was verified through survival analysis, risk curve, independent prognostic analysis, receiver operating characteristic (ROC) curve, difference analysis between high- and low-risk groups, and clinical correlation analysis. And to determine whether PRLncs-score is independent prognostic factor for OS. In addition, we further conducted external and internal validation for the risk prognosis model. Further analyses of immune cell infiltration and tumor microenvironment were performed. A pyroptosis-related competitive endogenous RNA (PRceRNA) network was constructed to obtain PRceRNAs associated with the prognosis of OS and performed gene set enrichment analysis (GSEA) on PRceRNA genes.

Results: We obtained five PRGs (CHMP4C, BAK1, GSDMA, CASP1, and CASP6) that predicted OS prognosis and seven PRLncs (AC090559.1, AP003119.2, CARD8-AS1, AL390728.4, SATB2-AS1, AL133215.2, and AC009495.3) and one PRceRNA (CARD8-AS1-hsa-miR-21-5p-IL1B) that predicted OS prognosis and indicated characteristics of the OS immune microenvironment. The PRLncs-score, in combination with other clinical features, was established as an independent prognostic factor for OS patients. Subsequent scrutiny of the tumor microenvironment and immune infiltration indicated that patients with low-PRLncs-scores were associated with reduced metastatic risk, improved survival rates, heightened levels of immune cells and stroma, and increased immune activity compared to those with high-PRLncs-scores.

Conclusion: The study's findings offer insight into the prognosis of OS and its immune microenvironment, and hold promise for improving early diagnosis and immunotherapy.

* Corresponding author.
  E-mail address: sousou369@163.com (P. Xu).

1. Introduction

As most frequent primary bone cancer, osteosarcoma (OS), develops from mesenchymal cells and is characterized by a tumor that generates an osteoid matrix. Common symptoms of OS include localized pain, swelling, and limited joint mobility. OS typically affects long bones, with the distal femur, proximal tibia, and proximal humerus being the most commonly affected sites. Nevertheless, other bones can also be affected. Although OS is more prevalent in children and adolescents, it can also occur in people over the age of 50, resulting in a second peak incidence [1,2]. OS affects 2–3 individuals per million each year in the general population. However, in the 15–19 age range, the annual incidence increases to 8–11 per million each year. Furthermore, OS constitutes about 15 % of all extracranial solid tumors in this age range, and is approximately 1.4 times more prevalent in males than in females [3]. Furthermore, OS can locally invade and metastasize early, most often to the lungs but also to bones and rarely to the lymph nodes; 30–50 % of the affected population develops recurrent disease [4]. The majority of cancer hospitals currently use neoadjuvant chemotherapy, extensive tumor resection, and further adjuvant chemotherapy to treat high-grade OS. Low-grade OS is usually treated only with surgical excision [1]. Localized disease in children and young adults boasts a five-year survival rate of 78 %. However, the same cannot be said for patients with recurrent and metastatic OS, whose five-year survival rate is a mere 20 % [2,5]. Over the past few decades, there has been a significant improvement in the survival rates of patients diagnosed with non-metastatic OS. However, the same cannot be said for patients diagnosed with metastatic OS, as their survival rates have not shown a similar level of improvement [6]. OS remains a significant health hazard, and additional research on its pathogenesis is necessary to establish novel therapeutic approaches that can enhance the overall survival rate among OS patients.

Pyroptosis, also referred to as cytoinflammatory necrosis, is a recently identified type of programmed cell death [7]. Unlike apoptosis, pyroptosis can lead to the activation and release of various danger-signal molecules and cytokines, this results in a robust inflammatory response and immune system activation [8]. Pyroptotic cells form numerous vesicles that form stomata in the cell membrane. These facilitate the release of inflammatory cytokines, specifically IL-1β and IL-18. Furthermore, the formation of stomata in the plasma membrane typically leads to membrane lysis, and thus the release of cytoplasmic components into the extracellular space, which causes nuclear condensation and cell enlargement [9,10]. Initially identified as a key mechanism of anti-infection, pyroptosis has now been found to play a significant role in tumors [9]. Inflammatory vesicles, gasdermin proteins, and pro-inflammatory cytokines, which are related to the occurrence, invasion, and metastasis of tumors, are key components of pyroptosis [11]. Huaier extract can promote pyroptosis that is mediated by NLRP3 and prevent the growth of non-small cell lung cancer [12]. Breast cancer tumor grade, tumor size, clinical stage, and risk of mortality are all adversely linked with the expression of
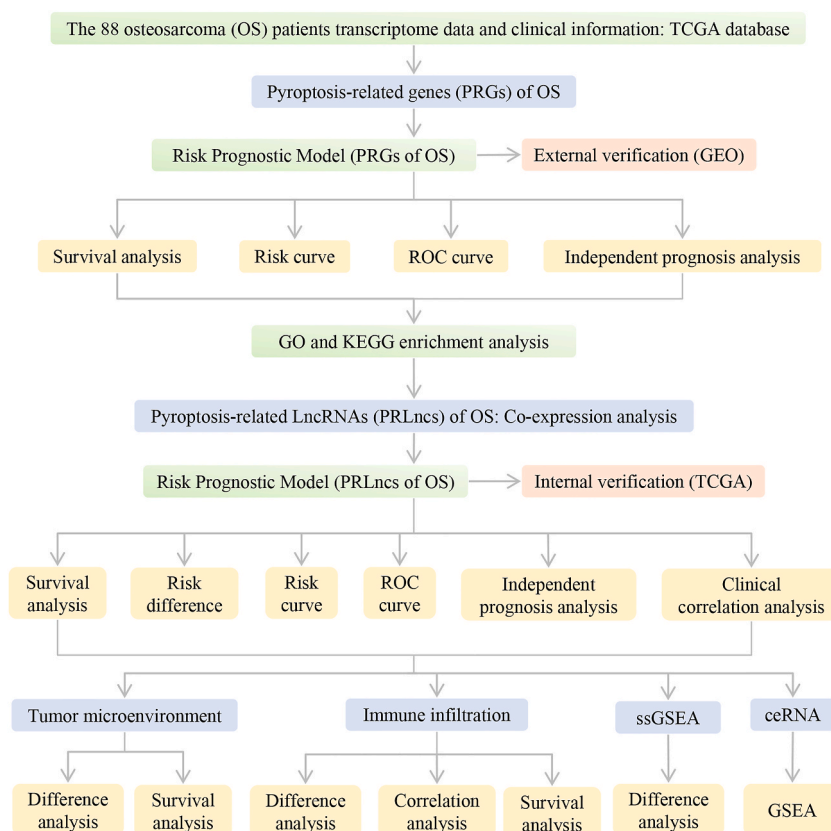

Fig. 1. Flow chart of this study.

pyroptosis-related proteins (CASP1, IL-1, and GSDMD) [13]. Pyroptosis and OS are tightly connected, according to earlier studies. The OS prognosis may be aided by pyroptosis-related long non-coding RNAs (PRLncs) associated with the OS microenvironment, includes RPARP-AS1, AC009159.3, and AC124312.3 [14]. By stress-activating the endoplasmic reticulum, physcion 8-*O*-beta-glucopyranoside causes NLRP3-related pyroptosis and promotes cell metastasis in human OS cells [15]. While studies have established a correlation between pyroptosis and OS, the precise role of this process in the development of OS is yet to be fully understood. Conducting additional research to explore the potential significance of pyroptosis in OS could be crucial in enhancing the survival rates of individuals affected by this condition.

Transcriptome and microarray analyses have proven to be valuable tools in the study of various diseases, such as tumors. These methods are utilized to identify novel biomarkers that can aid in the diagnosis, treatment, and prognosis of the disease [16,17]. In recent years, the use of bioinformatics in data mining has greatly advanced our understanding of the molecular mechanisms of disease, particularly in the field of cancer research. By identifying potential biomarkers, this analysis has also opened up new avenues for designing effective treatment strategies [18,19]. According to bioinformatics analysis, OLFML2B overexpression may serve as a promising diagnostic and prognostic marker for gastric cancer [20]. In a study aimed at developing a prognostic model for colon cancer, researchers have identified three autophagy markers (MAP1LC3C, WIPI2, and RAB7A) that are associated with the prognosis of colon cancer patients [21]. In addition to its role as an independent prognostic factor of OS patients, KIF21B has been shown to regulate tumor formation in vivo by modulating the PI3K/AKT pathway, specifically, downregulation of KIF21B has been found to inhibit cell proliferation and reduce tumor growth [22].

The transcriptome and clinical information of 88 OS patients from the Cancer Genome Atlas (TCGA) (https://portal.gdc.cancer.gov/) were utilized in this work to examine the association of pyroptosis-related genes (PRGs) and PRLncs in OS prognosis. Using this data, risk prognostic model was developed, and the risk score was calculated to predict OS survival. Additionally, investigating the association between the PRLncs-score and the tumor microenvironment and immunity may offer insights into the link between pyroptosis and immunotherapy response of OS patients. Fig. 1 presents a workflow chart of this study.

2. Materials and methods

2.1. Data download and arrangement

The transcriptome and clinical information for 88 OS cases was retrieved from the TCGA database. The clinical information comprised the following: the futime, fustat, gender, age at diagnosis in days, the disease at diagnosis (whether it was metastatic or not), the primary tumor site, and the specific tumor site. Two samples were removed because of incomplete survival data, and the remaining 86 samples were used for subsequent analysis.

2.2. PRGs related to OS prognosis

The OS transcriptome data contained both genes and lncRNAs. We identified 52 potential PRGs from previous reviews and intersected them with genes from the OS transcriptome data [9,23–27]. This process resulted in an OS-related PRGs expression matrix. Using Perl, we merged this matrix with survival data and performed univariate Cox regression analysis with the "survival" package in R. This allowed us to identify statistically significant PRGs that related to the OS prognosis [28].

2.3. Risk prognostic model of OS prognostic PRGs

A risk prognostic model of OS prognostic PRGs was built and optimized using "survival" package in R through multivariate stepwise Cox regression analysis. The risk score was determined: Risk score $= \sum_{i=1}^{n}(geneexp_i \times coef_i)$, where n denotes the total number of OS prognostic PRGs, i denotes the ith gene, and coef denotes the regression coefficient. The sample risk score (PRGs-score) was calculated by multiplying the expression of OS prognostic PRGs by the regression coefficient and added them. Based on the median, the samples were split into high- and low-risk groups.

2.4. Validation of the risk prognostic model of OS prognostic PRGs

In order to determine the survival difference in the high- and low-risk groups of the model, survival curves were created using the R "survival" and "survminer" packages. The variations in risk score, survival time, and OS prognostic PRGs in the high- and low-risk groups can then be observed by creating the risk curve, survival status map, and risk heatmap by R [29]. Clinical data and risk values are combined in Perl, and the "survival" package performed independent prognosis tests through Cox regression analyses both univariate and multivariate, to verify the model's independent prognostic ability [30]. The "survival," "survminer," and "timeROC" packages plot both receiver operating characteristic (ROC) curves of the risk score and clinical traits, as well as time-dependent ROC curves [21,29]. The accuracy of the model was evaluated using the area under the curve (AUC).

2.5. Enrichment analysis of OS prognostic PRGs

Enrichment analyses of OS prognostic PRGs in risk prognostic model were conducted using the R package "clusterProfiler", include

Gene Ontology (GO) and Kyoto Encyclopedia of Genes and Genomes (KEGG) enrichment analyses [21]. GO enrichment was assessed based on three dimensions: biological process (BP), cellular component (CC), and molecular function (MF).

2.6. OS-related PRLncs

To identify OS-related PRLncs, we utilized the "limma" package for co-expression analysis of OS prognostic PRGs in risk prognostic model and lncRNA in OS transcriptome data. The screening criteria consisted of a Pearson correlation coefficient > 0.5 and $P < 0.001$ [31].

2.7. PRLncs related to OS prognosis

After the expression matrix of OS-related PRLncs was obtained via co-expression analysis, Perl was used to merge it with the survival data. The "survival" package afforded the statistically significant PRLncs connected to OS prognosis via univariate Cox regression analysis [28].

2.8. Risk prognostic model of OS prognostic PRLncs

A risk prognostic model of OS prognostic PRLncs was built and optimized using "survival" package in R through multivariate stepwise Cox regression analysis. The risk score was determined: Risk score $= \sum_{i=1}^{n} (lncrnaexp_i \times coef_i)$, where n denotes the total number of OS prognostic PRLncs, i denotes the ith PRLncs, and coef denotes the regression coefficient. The sample risk score (PRLncs-score) was calculated by multiplying the expression of OS prognostic PRLncs by the regression coefficient and added them. Based on the median, the samples were split into high- and low-PRLncs-score groups.

2.9. Validation of the risk prognostic model of OS prognostic PRLncs

In order to determine the survival difference in the high- and low- PRLncs-score groups of the model, survival curves were created using the R "survival" and "survminer" packages. In order to determine the difference in the high- and low-PRLncs-score groups, differential analysis was performed using the R the "reshape2" and "ggpubr" packages. The variations in risk score, survival time, and OS prognostic PRLncs between the high- and low-PRLncs-score groups can then be observed by creating the risk curve, survival status map, and risk heatmap in R. Clinical data and PRLncs-score are combined in Perl, and the "survival" package performed independent prognosis tests through Cox regression analyses both univariate and multivariate, to verify the model's independent prognostic ability. The "survival," "survminer," and "timeROC" packages plot both time-dependent ROC curves, as well as ROC curves for the PRLncs-score and clinical traits. The clinical traits were grouped as follows: gender was divided into female and male, age at diagnosis in days was divided into ≤ 5245 (14 years old) and > 5245 (14 years old); the disease at diagnosis was divided into metastatic and non-metastatic; the primary tumor site was categorized into two regions, namely upper limb and lower limb + pelvis. Moreover, the specific tumor site was also sub-divided into upper limb and lower limb + pelvis. Perl was used to merge the grouped clinical data and PRLncs-score, and the "beeswarm" package to detect whether the PRLncs involved in the PRLncs-score and clinical traits were correlated [21].

2.10. Further validation for the risk prognostic model

We constructed risk prognostic models for OS prognostic PRGs and PRLncs. To ascertain the prognostic efficacy of the risk prognostic model concerning OS in patient cohorts, we performed supplementary validation analyses. Initially, we acquired the GSE21257 dataset from the Gene Expression Omnibus (GEO) database (https://www.ncbi.nlm.nih.gov/geo/). This dataset encompassed 53 cases of OS, upon which we externally validated the prognostic PRGs-driven risk prognostic model for OS. Subsequently, employing the risk prognostic model established on OS prognostic PRLncs, we partitioned a cohort of 86 OS patients sourced from TCGA database into distinct training and testing subsets, thus executing an internal validation procedure. The computation of the risk score and the demarcation of subjects into high and low-risk categories were upheld in congruence with the aforementioned methodology.

2.11. Tumor microenvironment analysis

The "limma" and "estimate" packages were employed to compute the immune, stromal, and total scores of each OS patient (28). To investigate the potential difference in the tumor microenvironment scores between high- and low-PRLncs-score groups, the "limma" and "ggpubr" packages were utilized [32]. The patient samples were stratified into high- and low-score groups according to the median value of tumor microenvironment scores. The "limma," "survival," and "survminer" packages were employed to compare the difference in survival rates between the high- and low-score groups.

2.12. Immune-related analysis

Data on the 22 infiltrating immune cell-matrix of the OS transcriptome were obtained using the CIBERSORT software ("e1071," "parallel," and "preprocessCore" packages) in R [33]. Samples demonstrating a statistically significant difference (P < 0.05) in the immune cell-matrix were retained. The "barplot" function of R draws the expression histogram of the 22 immune cells in the high- and low-PRLncs-score groups, the "pheatmap" package draws the expression heatmap, and the "vioplot" package draws the violin diagram. The samples were segregated into two groups, namely high- and low-expression, according to the median value of immune cells, and the "limma," "survival," and "survminer" packages were used to compare whether immune cells had survival differences in the high- and low-expression groups. The "ggcorrplot" and "psych" packages were used to analyze the correlation of OS prognostic PRGs and PRLncs with 22 immune cells. The present study utilized the single-sample gene set enrichment analysis (ssGSEA) approach implemented in the "GSVA," "limma," and "GSEABase" packages to calculate enrichment scores of immune cell populations and functional categories in the OS transcriptome data. To analyze potential differences in immune cell type and function between the high- and low-PRLncs-score groups, we utilized the "limma," "reshape2," and "ggpubr" packages [32].
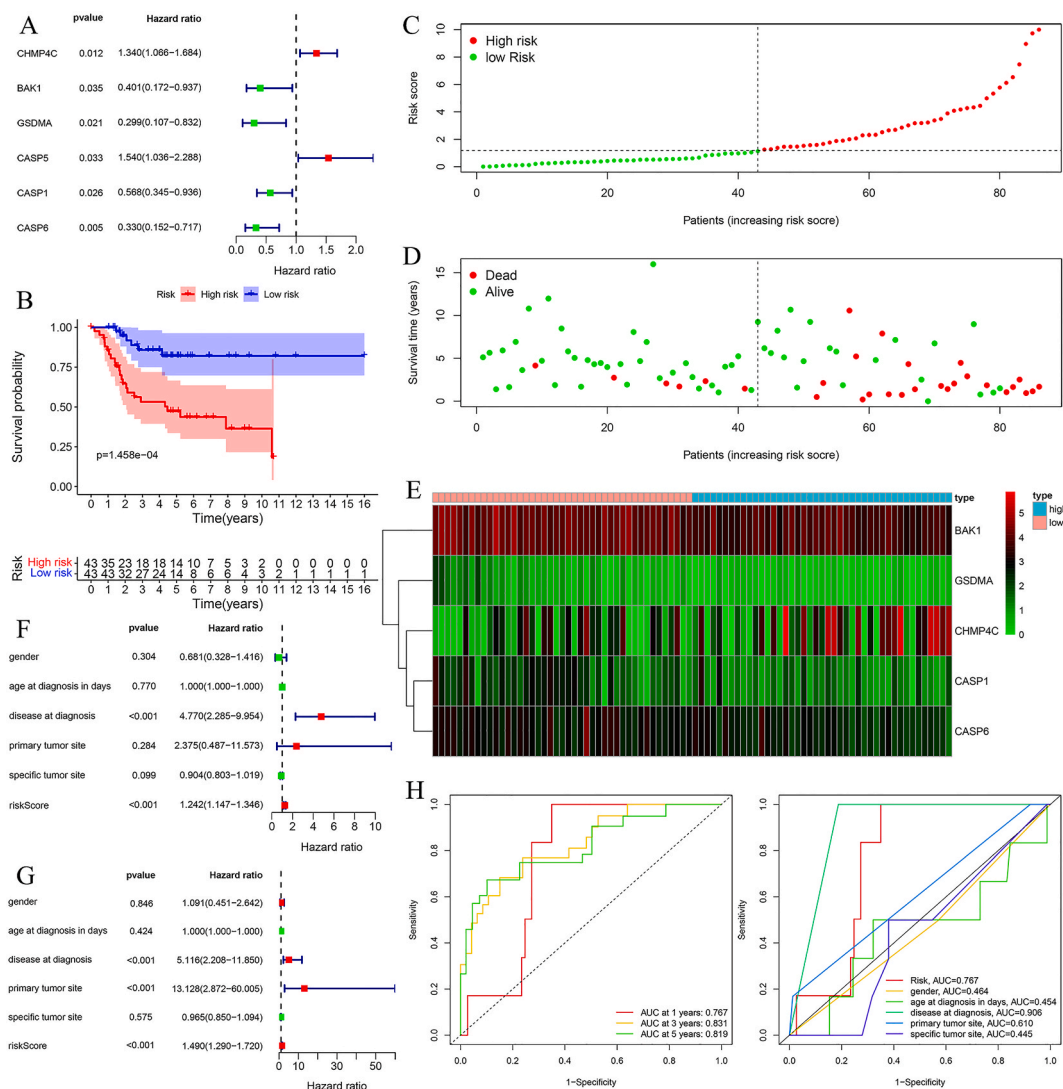
Fig. 2. Risk prognostic model of OS prognosis PRGs. (A) PRGs related to OS prognosis. (B) Survival curves in high- and low-risk groups. (C) Risk curves in high- and low-risk groups. (D) Survival status map in high- and low-risk groups. (E) Risk heatmap in high- and low-risk groups. (F) Univariate COX regression analysis. (G) Multivariate COX regression analysis. (H) Time-dependent ROC curves as well as ROC curves for risk score and clinical traits.

2.13. Construction of pyroptosis-related competitive endogenous RNAs (PRceRNAs) network related to OS prognosis

The ceRNA network was assembled utilizing the OS prognostic PRLncs in risk prognostic model. This method was employed to identify potential ceRNA interactions among the PRLncs. The starBase database predicted targeted microRNAs (miRNAs) of PRLncs. The TargetScan, miRTarBase, and miRDB databases predicted the target genes of miRNAs, the intersection of prediction results from three distinct databases was determined. The software tool Cytoscape was utilized to establish a ceRNA network. The genes in the ceRNA network were intersected with 52 PRGs, and PRceRNAs associated with the prognosis of OS were obtained based on the corresponding miRNAs and PRLncs of the intersected genes in the ceRNA network.

2.14. Gene set enrichment analysis (GSEA)

Genes in the OS prognosis-related PRceRNAs were further analyzed via GSEA, and P < 0.05 was established as the threshold for determining the statistical significance of the results. This analysis aimed to explore the biological pathways associated with OS prognosis and pyroptosis.

2.15. Statistical analysis

The statistical analyses were performed using R software version 4.0.5. The level of statistical significance was set at P < 0.05 unless otherwise specified.

3. Results

3.1. PRGs related to OS prognosis

Genes of the OS transcriptome data were intersected with the 52 PRGs, obtain the expression matrix of 52 OS-related PRGs. After merging with the survival data, six PRGs with statistical significance associated with the prognosis of OS were obtained via univariate Cox regression analysis. CASP5 and CHMP4C were identified as high-risk genes, whereas BAK1, GSDMA, CASP1, and CASP6 were low-risk genes (Fig. 2A).

3.2. Risk prognostic model of OS prognostic PRGs

A risk prognostic model of OS prognostic PRGs was constructed, and five OS prognostic PRGs (CHMP4C, BAK1, GSDMA, CASP1, and CASP6) were obtained after model optimization. After computing the sample's risk score using the established model formula, the sample was stratified into two groups: high-risk (N = 43) and low-risk (N = 43), according to the median values.

3.3. Validation of the risk prognostic model of OS prognostic PRGs

The survival curves indicate significant differences in the survival outcomes of the high-risk and low-risk cohorts, as evidenced by the five-year survival rates of 0.437 and 0.827, respectively (Fig. 2B). The results from the risk curve analysis indicated a gradual increase in the risk score of patients from the low-to the high-risk group (Fig. 2C). Based on the survival status chart, it is observed that there is a gradual decline in the survival rate of patients from the low-to the high-risk group, accompanied by a corresponding increase in mortality rate (Fig. 2D). The heatmap analysis of the risk assessment revealed a significant upsurge in the expression of CHMP4C gene in the high-risk group, indicating its classification as a high-risk gene, and a gradual increase in the expression of CHMP4C was observed from the low-risk to the high-risk group. The expression of BAK1, GSDMA, CASP1, and CASP6, which are low-risk genes, gradually decreased (Fig. 2E). Univariate independent prognostic analysis showed that the risk score and disease at diagnosis (metastatic or non-metastatic) could be used as independent prognostic factors, and they were both high-risk factors (Fig. 2F). Multivariate independent prognostic analysis showed that the risk score, disease at diagnosis (metastatic or non-metastatic), and the primary tumor site can serve as independent prognostic indicators and high-risk factors (Fig. 2G). The time-dependent ROC curve analysis demonstrated superior discriminatory performance of the PRG model in predicting overall survival prognosis at one, three, and five years, as evidenced by higher AUC, proving that the PRG model can predict the OS prognosis well. The ROC curve demonstrated that the risk score, disease at diagnosis (metastatic or non-metastatic), and the primary tumor site can serve as a prognostic factor for patient survival to a certain degree. The AUC for the risk score surpassed that of the overall clinical traits, suggesting that the risk prognostic model is a more precise predictor of patient survival than the clinical traits (Fig. 2H). The above results illustrate the accuracy of the PRG risk prognostic model for OS.

3.4. Enrichment analysis of OS prognostic PRGs

Five OS prognostic PRGs (CHMP4C, BAK1, GSDMA, CASP1, and CASP6) were subjected to enrichment analysis. GO enrichment analysis demonstrated that the OS prognostic PRGs were significantly enriched in the pyroptosis, protein processing, interleukin-1 alpha production, fibroblast apoptosis, and programmed necrotic cell death in BP. Also, they were significantly enriched in the ESCRT III complex, inflammasome complex, inflammasome complex, multivesicular body, and integral component of the

mitochondrial membrane in CC, as well as in cysteine-type peptidase activity, peptidase activator activity involved in apoptosis, phosphatidylserine binding, modified amino acid binding, and heat shock protein binding in MF (Fig. 3A). In terms of signaling pathways, OS prognostic PRGs were significantly enriched in apoptosis, necroptosis, cytosolic DNA-sensing pathway, melanoma, C-type lectin receptor signaling pathway, NOD-like receptor signaling pathway, transcriptional misregulation in cancer, Kaposi sarcoma-associated herpesvirus infection, coronavirus disease, and miRNAs involved in cancer (Fig. 3B).

3.5. OS-related PRLncs

The 44 OS-related PRLncs were determined via co-expression analysis of PRGs in the OS prognostic PRGs model and lncRNAs in the OS transcriptome data.

### 3.6. PRLncs related to OS prognosis

The expression matrix of OS-related PRLncs was integrated with survival data. And subjected to univariate Cox regression analysis, the results revealed that 27 PRLncs exhibited significant association with OS prognosis, comprising of 22 PRLncs classified as high-risk and 5 PRLncs as low-risk (Fig. 4A).

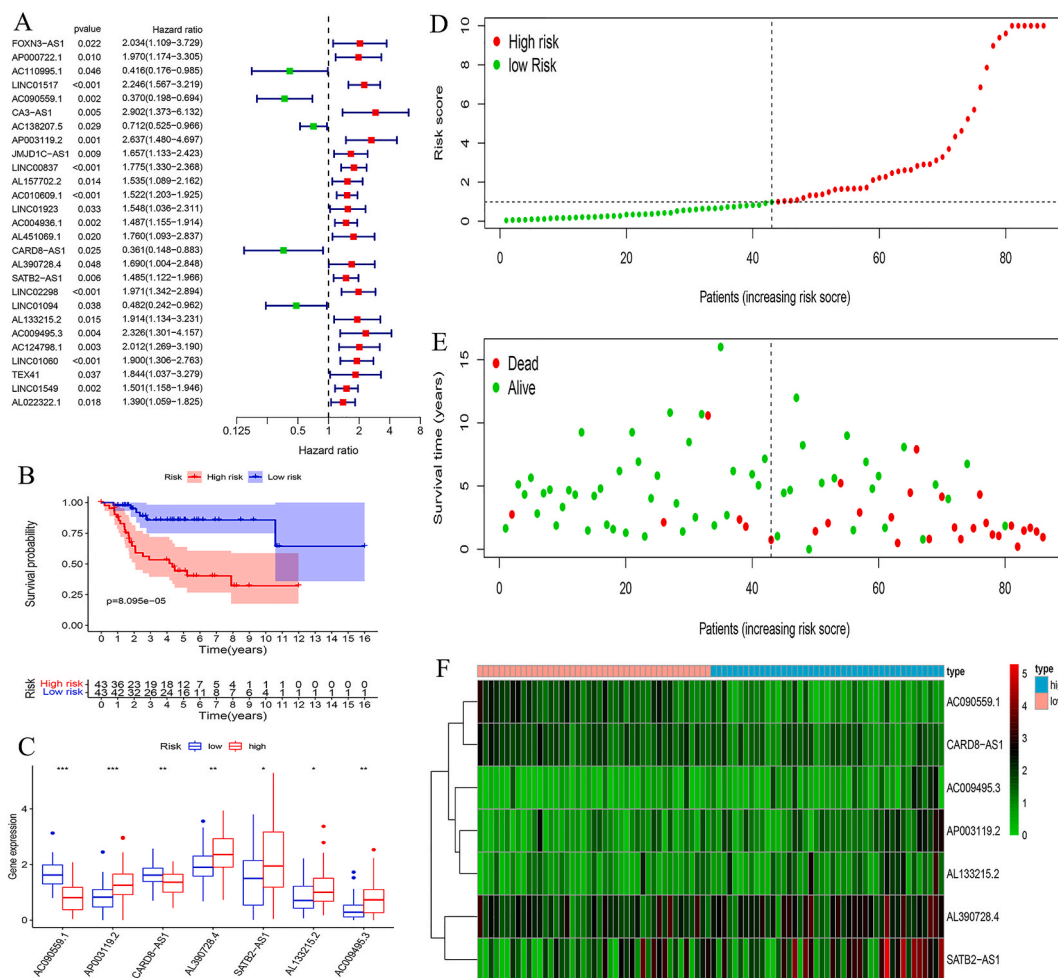### 3.7. Risk prognostic model of OS prognostic PRLncs

A risk prognostic model of PRLncs related to OS prognosis was constructed. After the model was optimized, seven OS-prognosis PRLncs (AC090559.1, AP003119.2, CARD8-AS1, AL390728.4, SATB2-AS1, AL133215.2, and AC009495.3) were obtained. The PRLncs-score for the sample was computed using the established model formula. According to the median, two groups were formed: a high-PRLncs-score group (N = 43) and a low-PRLncs-score group (N = 43).

3.8. Validation of the risk prognostic model of OS prognostic PRLncs

Based on the survival curve analysis, a significant difference in survival was observed between the groups with high- and low-PRLncs scores, as evidenced by their respective five-year survival rates of 0.403 and 0.858 (Fig. 4B). A total of seven OS prognostic PRLncs exhibited significant differences in the high- and low-PRLncs-score groups (Fig. 4C). The risk curve indicates a gradual increase in risk across the PRLncs-score groups, with a noticeable upward trend from the low-to the high-scoring groups (Fig. 4D). The survival status chart indicates a gradual decline in patient survival rates as the PRLncs-score group increases, accompanied by a corresponding increase in mortality rates (Fig. 4E). The risk heatmap showed that the expression of AP003119.2, AL390728.4, SATB2-AS1, AL133215.2, and AC009495.3, which were high-risk PRLncs, gradually increased from the low-to the high-PRLncs-score group. The expression of AC090559.1 and CARD8-AS1, which were low-risk PRLncs, gradually decreased (Fig. 4F). Based on both univariate and multivariate independent prognostic analyses, it has been determined that the PRLncs-score and disease status at the time of diagnosis (metastatic or non-metastatic) are viable independent prognostic factors, with both being deemed high-risk factors (Fig. 5A and B). The time-dependent ROC curve indicated that the AUC for the one-year, three-year, and five-year was comparatively higher, proving that the PRLncs-score can predict OS well. The ROC curve showed that the PRLncs-score, disease at diagnosis (metastatic or non-metastatic), and primary tumor site could predict patient survival to some extent. The AUC of the PRLncs-score was larger than that of the overall clinical traits, indicating that the PRLncs-score can better predict patient survival than clinical traits (Fig. 5C). Correlation analysis between PRLncs participating in the PRLncs-score and the clinical traits showed that AC090559.1 was significantly correlated with disease at diagnosis (metastatic or non-metastatic), primary tumor site, and specific tumor site, and its expression was higher in non-metastatic and lower limb + pelvis OS. The PRLncs-score was significantly correlated with disease at
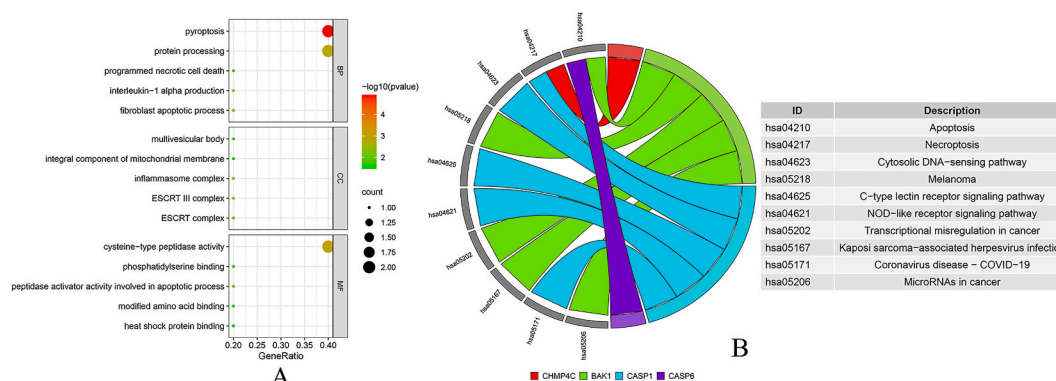
Fig. 3. Enrichment analysis of PRGs in the risk prognostic model. (A) GO enrichment analysis, including biological process, cellular component and molecular function. (B) KEGG enrichment analysis.

Fig. 4. Risk prognostic model of OS prognosis PRLncs. The risk score in the model was defined as PRLncs-score to predict OS survival. (A) PRLncs related to OS prognosis. (B) Survival curves in high- and low-PRLncs-score groups. (C) Risk difference analysis in high- and low-PRLncs-score groups. (D) Risk curves in high- and low-PRLncs-score groups. (E) Survival status map in high- and low-PRLncs-score groups. (F) Risk heatmap in high- and low-PRLncs-score groups.

diagnosis (metastatic or non-metastatic), and the PRLncs-score was higher in metastatic OS (Fig. 5D).

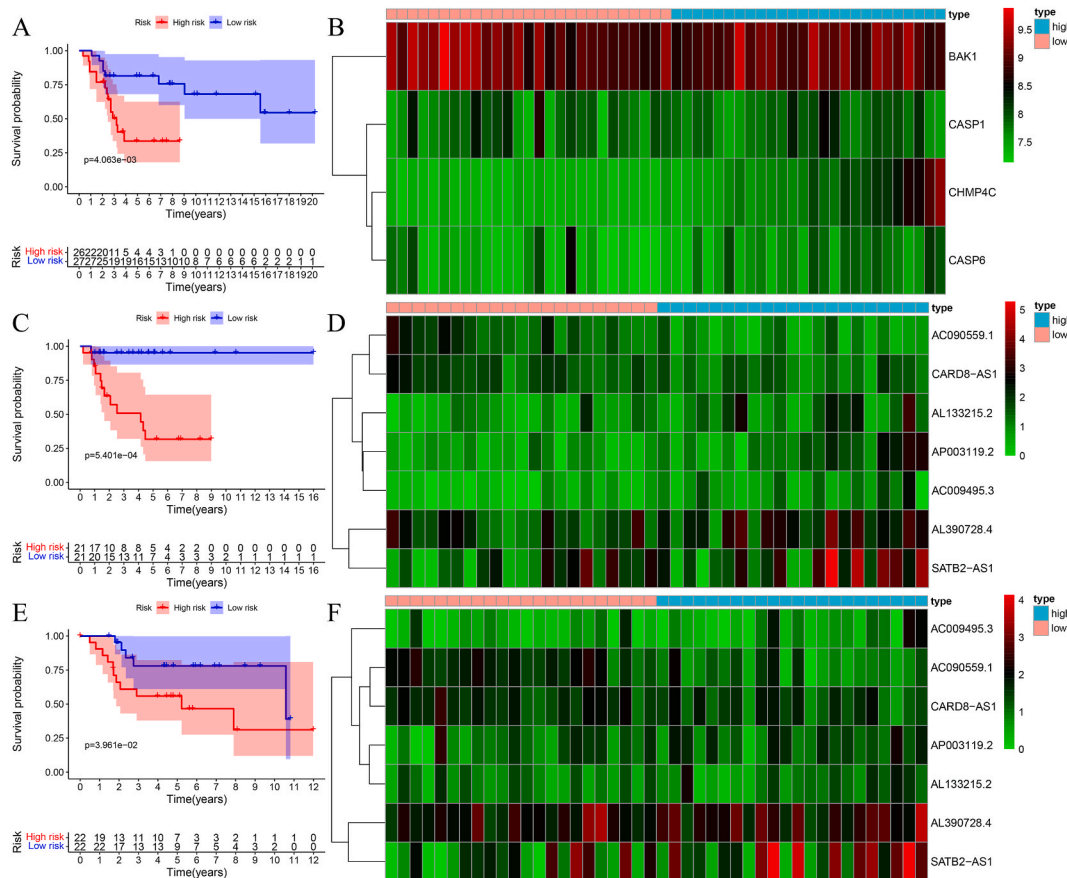### 3.9. Further validation for the risk prognostic model

The prognostic risk model for OS prognostic PRGs consists of a set of five PRGs: CHMP4C, BAK1, GSDMA, CASP1, and CASP6. However, within the GSE21257 dataset, only four PRGs (CHMP4C, BAK1, CASP1, and CASP6) manifest. Consequently, the external validation of the OS prognostic PRGs' risk model encompasses solely these aforementioned four PRGs. The outcomes derived from the survival analysis distinctly display noteworthy survival disparities between cohorts classified as high risk and low risk (Fig. 6A). This divergence is further underscored by the risk heatmap, which effectively illustrates variations in PRGs expression patterns between the high and low risk groups (Fig. 6B). Similarly, the internal validation of the risk prognostic model of OS prognostic PRLncs yields concordant findings. Survival analyses conducted on both the training and testing subsets distinctly exhibit substantial survival discrepancies (Fig. 6C and E). Correspondingly, the risk heatmap for PRLncs accentuates discernible distinctions in expression patterns between the high and low risk groups (Fig. 6D and F).

3.10. Tumor microenvironment analysis

There was a statistically significant increase in the scores of stromal and immune cells, as well as the total score of stromal and immune cells, in the low-PRLncs-score group compared to the high-PRLncs-score group (Fig. 7A). There were observed variations in survival rates among stromal and immune cells between high- and low-scoring groups; however, the total score of said cells did not display any significant disparity (Fig. 7B).
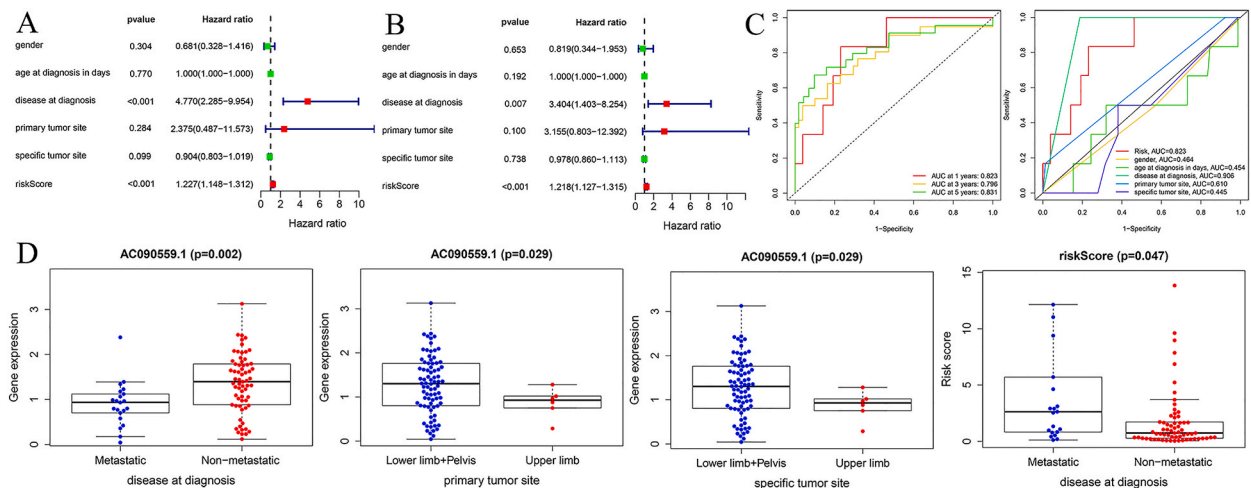
Fig. 5. Risk prognostic model of OS prognosis PRLncs. The risk score in the model was defined as PRLncs-score to predict OS survival. (A) Univariate COX regression analysis. (B) Multivariate COX regression analysis. (C) Time-dependent ROC curves as well as ROC curves for PRLncs-score and clinical traits. (D) Clinical correlation analysis.

Fig. 6. Internal and external validation of risk prognosis models. (A) External validation for the risk prognostic model of OS prognostic PRGs: survival analysis; (B) External validation for the risk prognostic model of OS prognostic PRGs: risk heatmap; (C) Internal validation for the risk prognostic model of OS prognostic PRLncs: survival analysis of the training group; (D) Internal validation for the risk prognostic model of OS prognostic PRLncs: risk heatmap of the training group; (E) Internal validation for the risk prognostic model of OS prognostic PRLncs: survival analysis of the testing group; (F) Internal validation for the risk prognostic model of OS prognostic PRLncs: risk heatmap of the testing group.
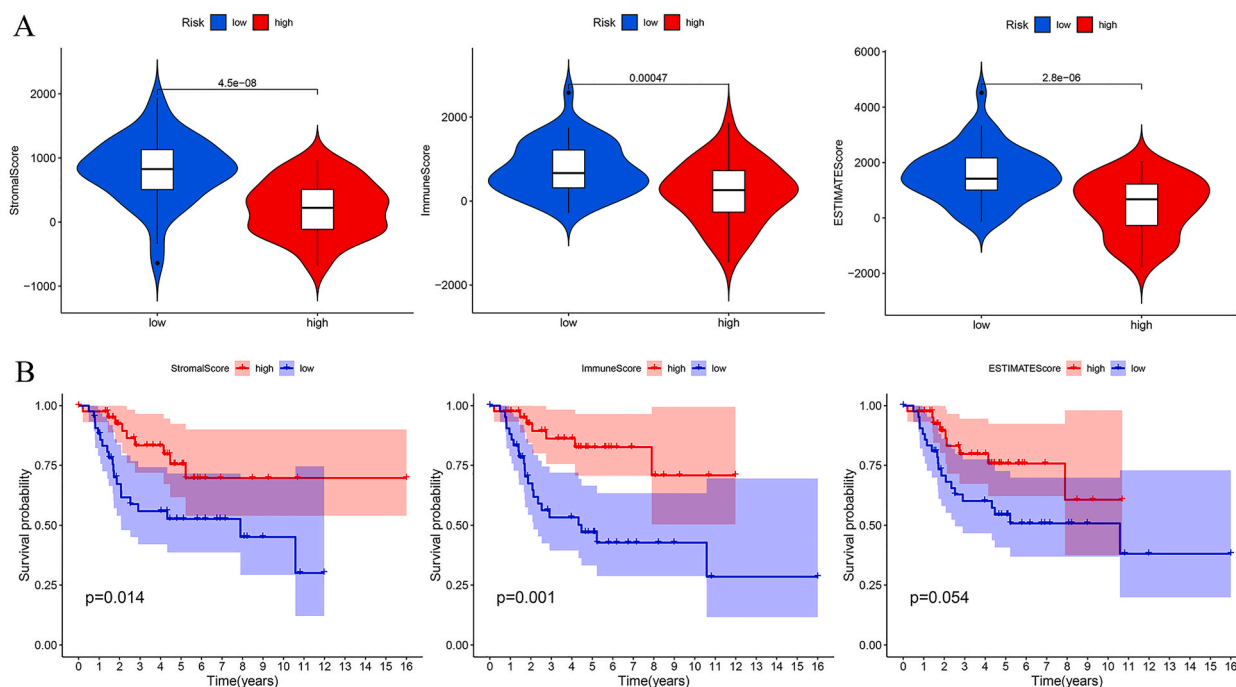
Fig. 7. Tumor microenvironment analysis. The risk score in the model was defined as PRLncs-score to predict OS survival. (A) The differential analysis of the scores of stromal cells and immune cells, and the total scores of stromal cells and immune cells in high- and low-PRLncs-score groups. (B) Analysis of survival differences of the scores of stromal cells and immune cells, and the total scores of stromal cells and immune cells between high and low score groups of the tumor microenvironment.

3.11. Immune-related analysis

The present study conducted an analysis of immune infiltrating cells in the high- and low-PRLncs-score groups. Specifically, we created both an expression histogram (Fig. 8A) and heatmap (Fig. 8B) to visualize, the results indicate that the expression of CD4 memory resting T cells, resting dendritic cells, resting NK cells, memory B cells, and activated dendritic cells was higher in the high-PRLncs-score group, whereas that of activated CD4 memory T cells was lower. Violin plots indicate that activated CD8 and CD4 memory T cells had significant differences in the high- and low-PRLncs-score groups. CD8 T cells were highly expressed in the high-PRLncs-score group and were a high-risk factor for OS. Activated CD4 memory T cells were weakly expressed in the high-PRLncs-score group and were a low-risk factor for OS (Fig. 8C). The samples were categorized into high- and low-expression groups, utilizing the median value of immune cells as the discriminatory threshold. Survival difference analysis revealed that resting mast cells, monocytes, plasma cells, and activated CD4 memory T cells showed survival differences of the high- and low-expression groups (Fig. 8D). A correlation analysis was conducted between OS prognostic PRGs and immune cells; the figure shows only the statistically significant correlation coefficients. The results of the study demonstrate a positive correlation between Macrophages M1 and M2 and CASP1, as well as a negative correlation between memory B cells and CHMP4C (Fig. 9A). Correlation analysis between the PRLncs involved in the PRLncs-score and immune cells was performed; the figure shows only the correlation coefficients with statistical significance. Macrophages M2 were positively correlated to AC090559.1 and CARD8-AS1, and macrophage M0 was negatively correlated to CARD8-AS1 (Fig. 9B). Based on the ssGSEA analysis, it was observed that the high-PRLncs-score group of patients exhibited a comparatively lower immune cell content in comparison to the low-PRLncs-score group (Fig. 9C), and immune functions were downregulated (Fig. 9D).

3.12. Construction of PRceRNAs network related to OS prognosis

Among the seven PRLncs involved in the PRLncs-score, three (CARD8-AS1, SATB2-AS1, and AL133215.2) predicted a total of 22 miRNAs in the starBase database. A total of 306 target genes were predicted from the 22 miRNAs. The software tool, Cytoscape, was employed to build a ceRNA network (Fig. 10A). The 306 target genes in the ceRNA network were intersected with 52 PRGs to obtain one gene (IL1B) (Fig. 10B). Based on the corresponding miRNAs and lncRNAs of IL1B in the ceRNA network, we identified a PRceRNA associated with the prognosis of OS (CARD8-AS1-hsa-miR-21-5p-IL1B).
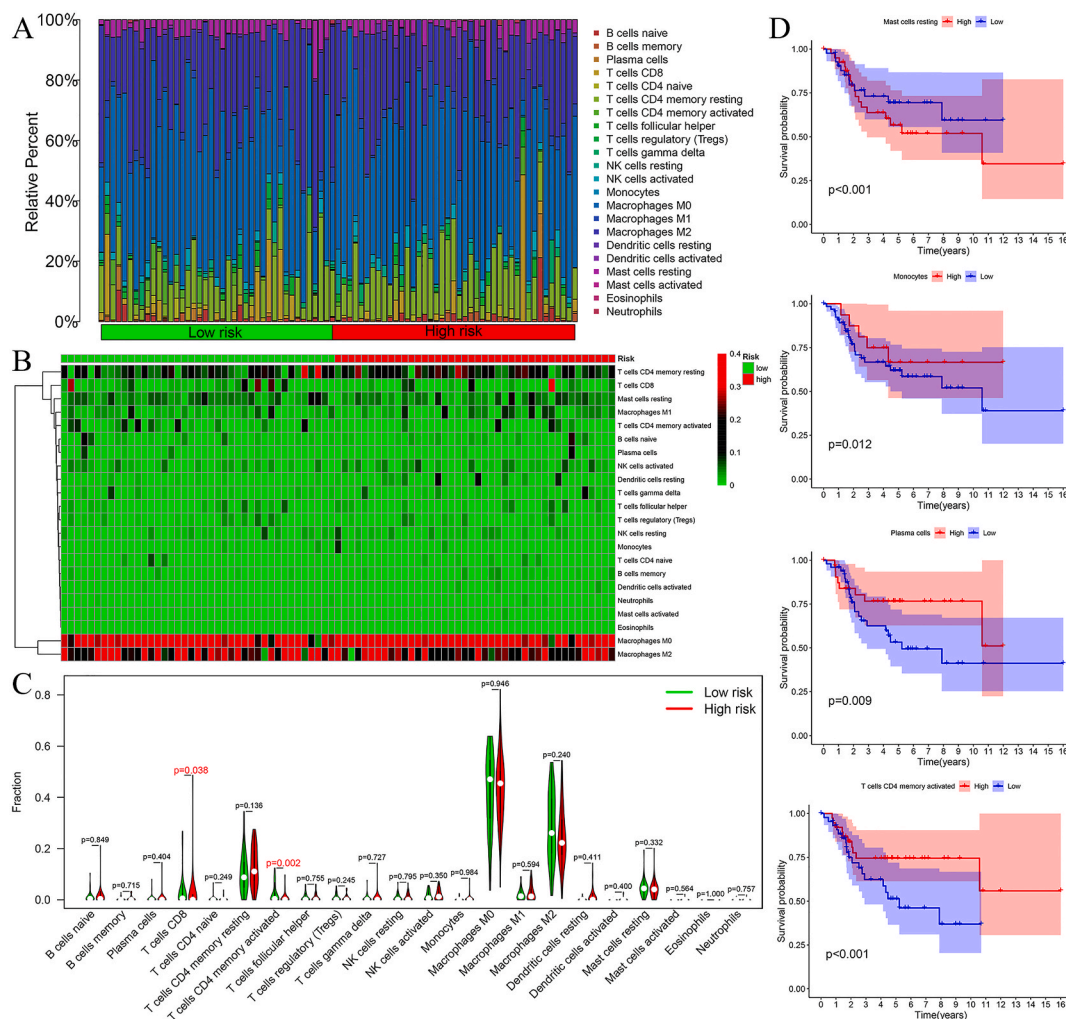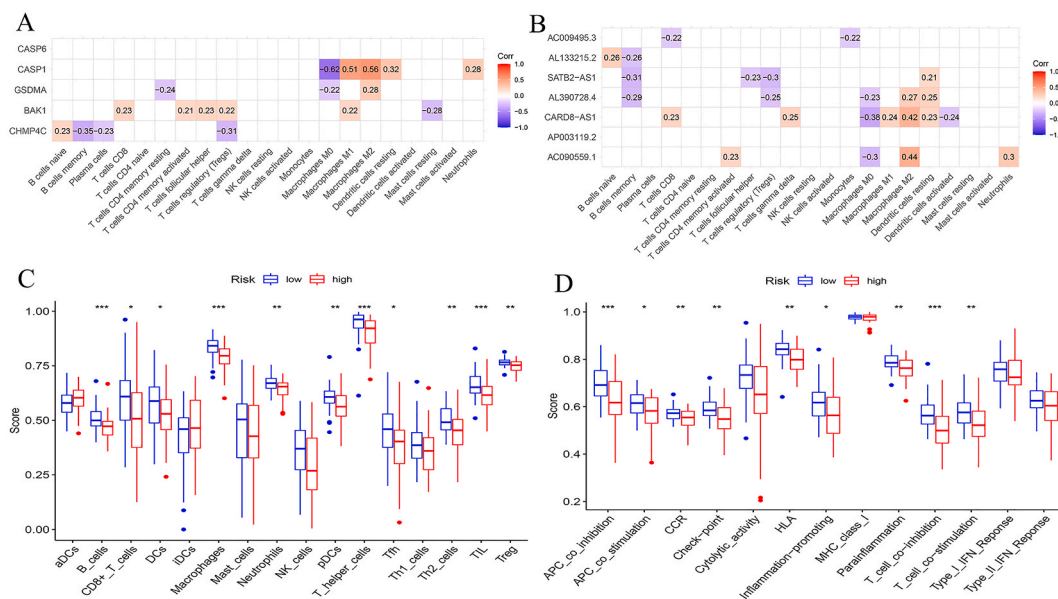
Fig. 8. Immune cells infiltrating. The risk score in the model was defined as PRLncs-score to predict OS survival. (A) Expression histogram of the immune cells in the high- and low-PRLncs-score groups. (B) Expression heatmap of the immune cells in the high- and low-PRLncs-score groups. (C) Violin diagram of the immune cells in the high- and low-PRLncs-score groups. (D) Analysis of survival differences of the immune cells between high and low score groups of the immune cells infiltrating.

3.13. GSEA

GSEA enrichment analysis of IL1B showed that it was enriched in the calcium, ERBB, Hedgehog, JAK-STAT, MAPK, p53, transforming growth factor-β (TGF-β), and Wnt signaling pathways (Fig. 11). These biological pathways may be closely associated with the prognosis and pyroptosis of OS patients.

4. Discussion

We used OS transcriptome and clinical data obtained from the TCGA database, a PRG prognostic model for OS was constructed through bioinformatics analysis. Based on the PRGs in the OS PRG prognostic model, the OS PRLncs were obtained via the co-expression method, the prognostic model for OS PRLncs was constructed, resulting in the PRLncs-score. Finally, we obtained five PRGs (CHMP4C, BAK1, GSDMA, CASP1, and CASP6) that could predict OS survival and seven PRLncs (AC090559.1, AP003119.2, CARD8-AS1, AL390728.4, SATB2-AS1, AL133215.2, and AC009495.3) that could predict OS prognosis and indicate immune microenvironmental characteristics. The verification process was conducted to assess the accuracy of the model via survival analysis, risk curve, independent prognostic analysis, ROC curve, difference analysis in the high- and low-PRLncs-score groups, and clinical correlation analysis; our investigation yielded that the PRLncs-score holds potential as an independent prognostic factor of the OS patient. More importantly, we further determined the prognostic value of the risk prognostic models of PRG and PRLncs for patients with OS through external and internal validation. After conducting a detailed analysis to the tumor microenvironment, as well as

Fig. 9. Immune correlation analysis and ssGSEA. The risk score in the model was defined as PRLncs-score to predict OS survival. (A) Correlation analysis of OS prognosis PRGs in risk prognostic model with immune cells. (B) Correlation analysis of OS prognosis PRLncs participating in the PRLncs-score with immune cells. (C) The differential analysis of the immune cells between high- and low-PRLncs-score groups. (D) The differential analysis of the immune function between high- and low-PRLncs-score groups.
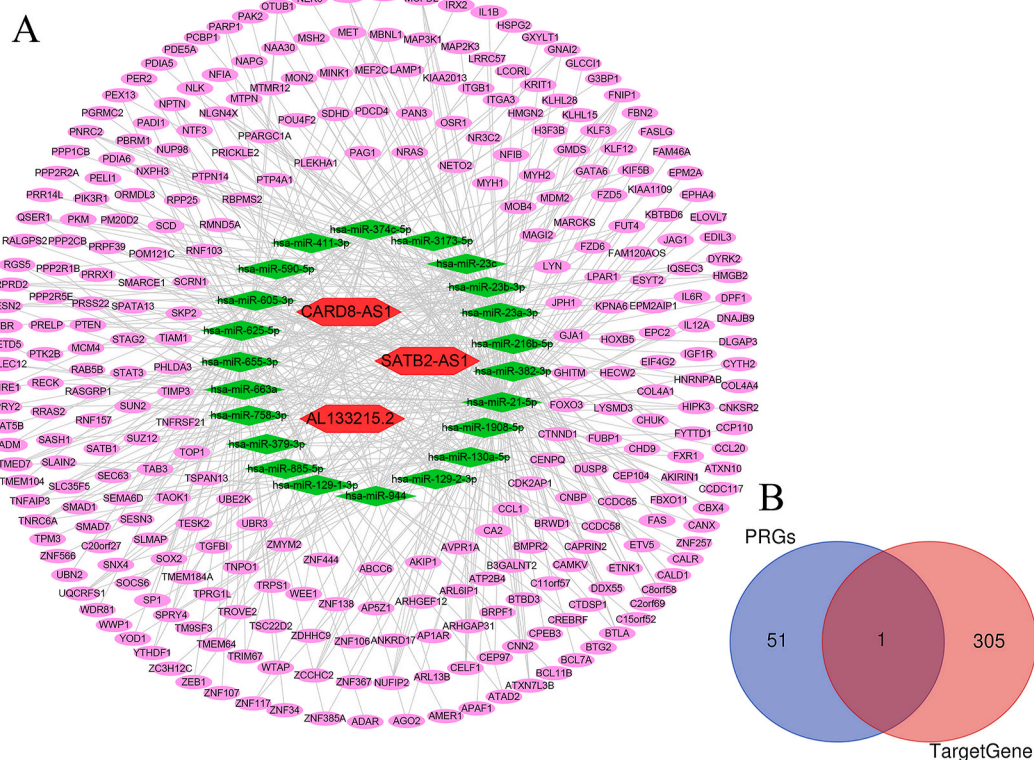
Fig. 10. CeRNAs network. (A) The ceRNAs network was constructed based on the PRLncs participating in the PRLncs-score. (B) The target genes in the ceRNAs network were intersected with 52 PRGs to obtain one gene (IL1B).
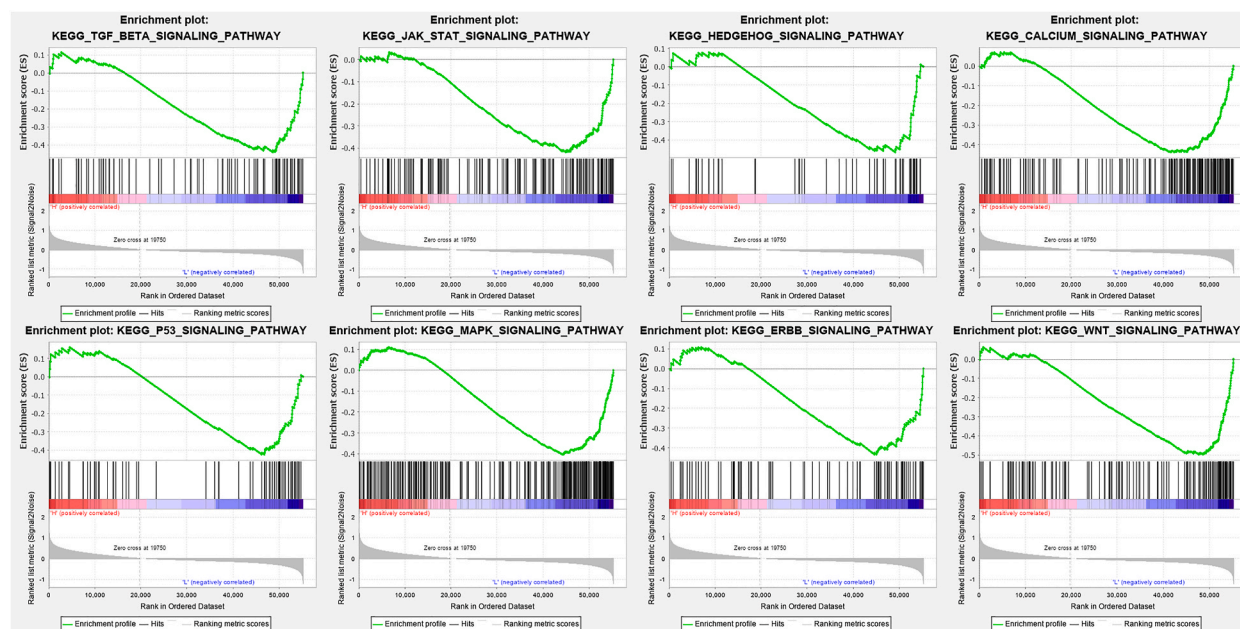
Fig. 11. GSEA enrichment analysis of the gene in OS prognosis-related PRceRNAs.

immune infiltration, we have identified that patients with a low PRLncs-score demonstrate a significantly lower risk of metastasis, a higher survival rate, and greater levels of immune cell and stromal content, as well as a more active immune function, in comparison to those with a high PRLncs-score. Furthermore, the analysis of immune cell infiltration indicated that the presence of CD8 T cells was strongly associated with a high risk of OS prognosis. Conversely, activated CD4 memory T cells were identified as a low-risk factor. Moreover, survival difference analysis demonstrated that the expression levels of resting mast cells, monocytes, plasma cells, and activated CD4 memory T cells differed significantly in the high- and low-expression groups, with implications for survival outcomes. By constructing a ceRNA network, we identified a PRceRNA related to OS prognosis (CARD8-AS1-hsa-miR-21-5p-IL1B).

A high-level transcriptome correlation study identified CHMP4C as a novel susceptibility gene and splice variant in serous epithelial ovarian cancer [34]. CHMP4C plays a crucial role in the promotion of cervical cancer cell viability by regulating the process of epithelial-mesenchymal transition, and CHMP4C could potentially serve as a novel biomarker for the early detection and diagnosis of cervical cancer [35]. The prognostic risk model utilizing autophagy-related genes has revealed that CHMP4C is a significant predictor of the prognosis of patients diagnosed with cervical cancer [30]. BAK1 is not only associated with apoptosis but also with pyroptosis [36]. The pathophysiology of heart failure involves complex molecular mechanisms, one of which is the inhibition of cardiomyocyte apoptosis by miR-125b through targeting BAK1 [37]. BAK1 is an autophagy-related gene that can predict OS prognosis [38]. In this study, we found that BAK1 may be a PRG for the prognosis of OS, which further confirmed the prognostic value of BAK1 in OS. GSDMA is expressed in epithelial cells and is associated with autoimmune diseases and cancer [39]. Furthermore, GSDMA initiates apoptosis (TGF-β), and transcription factor LMO1 upregulates GSDMA to promote apoptosis, resulting in decreased cell growth in gastric cancer [40,41]. As a PRG, GSDMA has been shown to have predictive value in assessing the prognosis of individuals with cutaneous melanoma [42]. CASP1 plays a pivotal role in facilitating the maturation and secretion of pro-inflammatory cytokines, namely IL-1β and IL-18, while simultaneously eliciting pyroptosis [24]. Diabetic retinopathy involves the dysregulation of lncRNA MIAT, which is known to modulate pyroptosis in primary human retinal cells, specifically, MIAT exerts its influence through regulating miR-342-3p that target CASP1 [43]. PRMT5 regulates pyroptosis in multiple myeloma cells by silencing CASP1 [44]. NOTCH3 and CASP1 have been identified as specific interaction pairs in OS, and are believed to potentially play a significant role in the pathogenesis and progression of the disease [45]. CASP6 is not only an apoptosis-related gene in hepatocellular carcinoma that predicts overall survival and response to immunotherapy [46], but also a pyroptosis-related prognostic gene in lung adenocarcinoma and glioma [47, 48]. Cisplatin specifically induces apoptosis in OS cells by activating CASP8, CASP3, and CASP6 [49]. Previous studies have shown that CHMP4C, BAK1, and CASP6 are PRGs for the prognosis of OS [32]. After careful analysis, it can be affirmed that the identified PRGs exhibit promising prognostic implications in terms of overall survival of OS. GSDMA and CASP1 were the other two PRGs associated with OS prognosis.

AC090559.1 is not only autophagy-related lncRNA that can predict lung adenocarcinoma survival [50] but also prognostic lncRNA associated with ferroptosis in the tumor microenvironment of lung adenocarcinoma [51]. Furthermore, in vitro metastatic capacity of glioma cell lines can be modulated by CARD8-AS1 [52], and Furthermore, in vitro metastatic capacity of glioma cell lines can be modulated by CARD8-AS1 [52], and CARD8-AS1 also can predict the survival prognosis of ovarian cancer [53]. SATB2-AS1 can act as a ferroptosis-related lncRNA and immune-related lncRNA with important prognostic value in lung adenocarcinoma [54,55]. Also, ATB2-AS1 is overexpressed in OS to promote cell proliferation and growth, and it is a new clinical feature that predicts OS recurrence

[56,57]. AP003119.2, AL390728.4, AL133215.2, and AC009495.3 have not been reported thus far; they may be PRLncs that predict OS prognosis, which can lead to a new research direction. miRNAs also play important roles in OS, and miR-191 and miR-195 are potential serum biomarkers for OS diagnosis, as well as prognosis [58,59]. The present study demonstrates that PWRN1 exhibits inhibitory effects on the proliferation and migration of glioblastoma cancer cells by regulating miR-21-5p expression in an inverse manner [60]. MiR-21-5p is also associated with tumor prognosis, and ceRNA (SNHG1-hsa-miR-21-5p-RALGPS2) may be a promising biomarker for predicting the prognosis and guiding treatment decisions for patients with lung adenocarcinoma [61]. Research in the field has demonstrated that IL1B exhibits differential expression in cases of metastatic OS [62], and IL1B gene polymorphisms are associated with OS risk [63]. Macrophages reduce OS sensitivity to neoadjuvant chemotherapeutics by secreting IL1B [64]. In this study, we discovered PRceRNA (CARD8-AS1-hsa-miR-21-5p-IL1B) associated with OS prognosis, which is greatly significant of the treatment and prognosis for parients with OS.

Prior research has investigated the relevant features that can predict OS survival from multiple perspectives. An autophagy-related clinical prognostic model identified autophagy-related genes associated with OS prognosis [65]. Key prognostic indicators for OS that can direct clinical decisions regarding OS treatment have been shown to be autophagy-related genes [38]. An OS prognostic model of hypoxia-related genes revealed that hypoxia in OS triggers immune cell death and improves the treatment [66]. A risk prognostic model of OS based on immune characteristics showed that TYROBP is a key immunomodulatory gene, which has important implications for the prognosis and immunotherapy of OS patients [67]. In the present study, we found PRGs that are associated with OS prognosis and derived PRLncs and PRceRNAs that predict OS prognosis and indicate immune microenvironment characteristics.

This study is subject to certain limitations. Firstly, the sample size was somewhat modest compared to those in other tumor studies. Secondly, the study's findings have not been experimentally validated, and the specific mechanisms in OS prognosis require further research.

5. Conclusion

In the present study, we identified five PRGs related to prognosis of OS patients, seven PRLncs, and one PRceRNA that can predict OS prognosis and indicate immune microenvironment characteristics via bioinformatics analysis. The obtained findings establish a basis for future investigations regarding the interplay between OS pyroptosis-associated indicators and immunity. Additionally, these results hold promising implications for enhancing the OS survival rate.

Ethics approval and consent to participate

Not applicable.

Consent for publication

All authors agree to publish the manuscript in this journal.

Data availability statement

The data associated with our study been deposited into a publicly available repository, named TCGA database (https://portal.gdc.cancer.gov/). The TCGA is a publicly available database that any researcher can use without requiring accession number.

Funding

Not applicable.

CRediT authorship contribution statement

Mingyi Yang: Formal analysis, Methodology, Writing – original draft, Writing – review & editing. **Haishi Zheng:** Data curation, Formal analysis, Methodology, Writing – original draft. **Yani Su:** Data curation, Formal analysis, Methodology. **Ke Xu:** Data curation, Resources. **Qiling Yuan:** Data curation, Resources. **Yongsong Cai:** Data curation, Resources. **Yirixiati Aihaiti:** Software, Visualization. **Peng Xu:** Conceptualization, Investigation, Project administration, Supervision.

Declaration of competing interest

The authors declare that they have no known competing financial interests or personal relationships that could have appeared to influence the work reported in this paper.

Acknowledgements

Not applicable.

References

[1] D.D. Moore, H.H. Luu, Osteosarcoma. Cancer Treat Res 162 (2014) 65–92.
[2] M. Kansara, et al., Translational biology of osteosarcoma, Nat. Rev. Cancer 14 (11) (2014) 722–735.
[3] J. Ritter, S.S. Bielack, Osteosarcoma. Annals of Oncology 21 (2010) vii320–vii325.
[4] S. Berhe, et al., Unusual abdominal metastases in osteosarcoma, Journal of Pediatric Surgery Case Reports 28 (2018) 13–16.
[5] N. Gaspar, et al., Results of methotrexate-etoposide-ifosfamide based regimen (M-EI) in osteosarcoma patients included in the French OS2006/sarcome-09 study, Eur. J. Cancer 88 (2018) 57–66.
[6] D.C. Allison, et al., A Meta-Analysis of Osteosarcoma Outcomes in the Modern Medical Era, Sarcoma, 2012, 704872, 2012.
[7] S.B. Kovacs, E.A. Miao, Gasdermins: effectors of pyroptosis, Trends Cell Biol. 27 (9) (2017) 673–684.
[8] R. Tang, et al., Ferroptosis, necroptosis, and pyroptosis in anticancer immunity, J. Hematol. Oncol. 13 (1) (2020).
[9] Y. Ye, Q. Dai, H. Qi, A novel defined pyroptosis-related gene signature for predicting the prognosis of ovarian cancer, Cell Death Dis. 7 (1) (2021) 71.
[10] P. Broz, P. Pelegrin, F. Shao, The gasdermins, a protein family executing cell death and inflammation, Nat. Rev. Immunol. 20 (3) (2020) 143–157.
[11] R. Kolb, et al., Inflammasomes in cancer: a double-edged sword, Protein & Cell 5 (1) (2014) 12–20.
[12] J. Xie, et al., Huaier extract suppresses non-small cell lung cancer progression through activating NLRP3-dependent pyroptosis, Anat. Rec. 304 (2) (2021) 291–301.
[13] X. Wu, et al., Detection of proteins associated with the pyroptosis signaling pathway in breast cancer tissues and their significance, Int. J. Clin. Exp. Pathol. 13 (6) (2020) 1408–1414.
[14] X. Bu, et al., Prognostic value of a pyroptosis-related long noncoding RNA signature associated with osteosarcoma microenvironment, JAMA Oncol. 2021 (2021), 2182761.
[15] B. Tian, et al., Retracted article: physcion 8-O-beta-glucopyranoside mediates the NLRP3-associated pyroptosis and cell metastasis in the human osteosarcoma cells via ER stress activation, Naunyn-Schmiedeberg's Arch. Pharmacol. 394 (3) (2021) 555.
[16] H.L. Carr, et al., New developments in transcriptomic analysis of synovial tissue, Front. Med. 7 (2020) 21.
[17] D. Demircioglu, et al., A pan-cancer transcriptome analysis reveals pervasive regulation through alternative promoters, Cell 178 (6) (2019) 1465–1477 e17.
[18] M.X. Li, et al., Identification of potential core genes in triple negative breast cancer using bioinformatics analysis, OncoTargets Ther. 11 (2018) 4105–4112.
[19] X. Lv, et al., Identification of potential key genes and pathways predicting pathogenesis and prognosis for triple-negative breast cancer, Cancer Cell Int. 19 (2019) 172.
[20] J. Liu, et al., Bioinformatic exploration of OLFML2B overexpression in gastric cancer base on multiple analyzing tools, BMC Cancer 19 (1) (2019) 227.
[21] T.T. Liu, S.M. Liu, Prediction of prognostic biomarkers and construction of an autophagy prognostic model for colorectal cancer using bioinformatics, Technol. Cancer Res. Treat. 19 (2020), 1533033820984177.
[22] S. Ni, et al., KIF21B expression in osteosarcoma and its regulatory effect on osteosarcoma cell proliferation and apoptosis through the PI3K/AKT pathway, Front. Oncol. 10 (2020), 606765.
[23] C.B. Zhou, J.Y. Fang, The role of pyroptosis in gastrointestinal cancer and immune responses to intestinal microbial infection, Biochim. Biophys. Acta Rev. Canc 1872 (1) (2019) 1–10.
[24] X. Xia, et al., The role of pyroptosis in cancer: pro-cancer or pro-"host"? Cell Death Dis. 10 (9) (2019).
[25] D. Wu, et al., Pyroptosis, a new breakthrough in cancer treatment, Front. Oncol. 11 (2021), 698811.
[26] L. Li, Y. Li, Y. Bai, Role of GSDMB in pyroptosis and cancer, Cancer Manag. Res. 12 (2020) 3033–3043.
[27] X. Ju, et al., Role of pyroptosis in cancer cells and clinical applications, Biochimie 185 (2021) 78–86.
[28] H. Qian, et al., Expression of lipid-metabolism genes is correlated with immune microenvironment and predicts prognosis in osteosarcoma, Front. Cell Dev. Biol. 9 (2021), 673827.
[29] P. Wu, et al., Identification and validation of a pyroptosis-related prognostic signature for thyroid cancer, Cancer Cell Int. 21 (1) (2021) 523.
[30] H. Shi, et al., Application of an autophagy-related gene prognostic risk model based on TCGA database in cervical cancer, Front. Genet. 11 (2020), 616998.
[31] Q. Fan, B. Liu, Identification of a RNA-seq based 8-long non-coding RNA signature predicting survival in esophageal cancer, Med. Sci. Mon. Int. Med. J. Exp. Clin. Res. 22 (2016) 5163–5172.
[32] Y. Zhang, et al., A novel pyroptosis-related signature for predicting prognosis and indicating immune microenvironment features in osteosarcoma, Front. Genet. 12 (2021), 780780.
[33] J.I. Kawada, et al., Immune cell infiltration landscapes in pediatric acute myocarditis analyzed by CIBERSORT, J. Cardiol. 77 (2) (2021) 174–178.
[34] A. Gusev, et al., A transcriptome-wide association study of high-grade serous epithelial ovarian cancer identifies new susceptibility genes and splice variants, Nat. Genet. 51 (5) (2019) 815–823.
[35] S.L. Lin, et al., Chromatin modified protein 4C (CHMP4C) facilitates the malignant development of cervical cancer cells, FEBS Open Bio 10 (7) (2020) 1295–1303.
[36] A.D. Cowan, et al., BAK core dimers bind lipids and can be bridged by them, Nat. Struct. Mol. Biol. 27 (11) (2020) 1024–1031.
[37] B. Zhang, et al., MiR-125b inhibits cardiomyocyte apoptosis by targeting BAK1 in heart failure, Mol. Med. 27 (1) (2021) 72.
[38] W. Qi, et al., Prognostic signature of osteosarcoma based on 14 autophagy-related genes, Pathol. Oncol. Res. 27 (2021), 1609782.
[39] P. Orning, E. Lien, K.A. Fitzgerald, Gasdermins and their role in immunity and inflammation, J. Exp. Med. 216 (11) (2019) 2453–2465.
[40] D. Sarrio, et al., The multifaceted roles of gasdermins in cancer biology and oncologic therapies, Biochim. Biophys. Acta Rev. Canc 1876 (2) (2021), 188635.
[41] S. Qiu, J. Liu, F. Xing, 'Hints' in the killer protein gasdermin D: unveiling the secrets of gasdermins driving cell death, Cell Death Differ. 24 (4) (2017) 588–596.
[42] X. Niu, et al., Construction and validation of a novel pyroptosis-related signature to predict prognosis in patients with cutaneous melanoma, Math. Biosci. Eng. 19 (1) (2021) 688–706.
[43] X. Yu, et al., Long noncoding RNA MIAT regulates primary human retinal pericyte pyroptosis by modulating miR-342-3p targeting of CASP1 in diabetic retinopathy, Exp. Eye Res. 202 (2021), 108300.
[44] T. Xia, et al., PRMT5 regulates cell pyroptosis by silencing CASP1 in multiple myeloma, Cell Death Dis. 12 (10) (2021) 851.
[45] H. Li, et al., Identification of characteristic gene modules of osteosarcoma using bioinformatics analysis indicates the possible molecular pathogenesis, Mol. Med. Rep. 15 (4) (2017) 2113–2119.
[46] S. Zheng, et al., Identification of a pyroptosis-related gene signature for predicting overall survival and response to immunotherapy in hepatocellular carcinoma, Front. Genet. 12 (2021).
[47] W. Lin, et al., Identification of the pyroptosisrelated prognostic gene signature and the associated regulation axis in lung adenocarcinoma, Cell Death Dis. 7 (1) (2021) 161.
[48] B. Chao, et al., Predicting the prognosis of glioma by pyroptosis-related signature, J. Cell Mol. Med. 26 (1) (2022) 133–143.
[49] K. Seki, et al., Cisplatin (CDDP) specifically induces apoptosis via sequential activation of caspase-8, -3 and -6 in osteosarcoma, Cancer Chemother. Pharmacol. 45 (3) (2000) 199–206.
[50] L. Wu, et al., A novel autophagy-related lncRNA survival model for lung adenocarcinoma, J. Cell Mol. Med. 25 (12) (2021) 5681–5690.
[51] Y. Guo, et al., Identification of a prognostic ferroptosis-related lncRNA signature in the tumor microenvironment of lung adenocarcinoma, Cell Death Dis. 7 (1) (2021) 190.
[52] X. Lin, et al., Characterization of transcriptome transition associates long noncoding RNAs with glioma progression, Mol. Ther. Nucleic Acids 13 (2018) 620–632.
[53] N. Li, X. Zhan, Identification of clinical trait-related lncRNA and mRNA biomarkers with weighted gene co-expression network analysis as useful tool for personalized medicine in ovarian cancer, EPMA J. 10 (3) (2019) 273–290.
[54] L. Lu, et al., Identification of a ferroptosis-related LncRNA signature as a novel prognosis model for lung adenocarcinoma, Front. Oncol. 11 (2021), 675545.

[55] Y. Chen, et al., Immune-related eight-lncRNA signature for improving prognosis prediction of lung adenocarcinoma, J. Clin. Lab. Anal. 35 (11) (2021), e24018.
[56] S.H. Liu, et al., A novel antisense long non-coding RNA SATB2-AS1 overexpresses in osteosarcoma and increases cell proliferation and growth, Mol. Cell. Biochem. 430 (1–2) (2017) 47–56.
[57] T. Ying, et al., The lncRNAs RP1-261G23.7, RP11-69E11.4 and SATB2-AS1 are a novel clinical signature for predicting recurrent osteosarcoma, Biosci. Rep. 40 (1) (2020).
[58] T. Wang, et al., Increased expression of microRNA-191 as a potential serum biomarker for diagnosis and prognosis in human osteosarcoma, Cancer Biomarkers 15 (5) (2015) 543–550.
[59] H. Cai, et al., Serum miR-195 is a diagnostic and prognostic marker for osteosarcoma, J. Surg. Res. 194 (2) (2015) 505–510.
[60] J. Jiang, X. Wang, J. Lu, PWRN1 suppressed cancer cell proliferation and migration in glioblastoma by inversely regulating hsa-miR-21-5p, Cancer Manag. Res. 12 (2020) 5313–5322.
[61] J. Tan, et al., Integrative analysis of three novel competing endogenous RNA biomarkers with a prognostic value in lung adenocarcinoma, BioMed Res. Int. 2020 (2020), 2837906.
[62] G.L. Capella, Adrenergic urticaria and rheumatoid arthritis in a patient with melanoma: an intricate medical management, J. Drugs Dermatol. JDD 11 (3) (2012) 409–412.
[63] Y. He, et al., Genetic polymorphisms of interleukin-1 beta and osteosarcoma risk, Int. Orthop. 38 (8) (2014) 1671–1676.
[64] X. Liang, et al., Macrophages reduce the sensitivity of osteosarcoma to neoadjuvant chemotherapy drugs by secreting Interleukin-1 beta, Cancer Lett. 480 (2020) 4–14.
[65] J. Li, et al., Establishment of an autophagy-related clinical prognosis model for predicting the overall survival of osteosarcoma, BioMed Res. Int. 2021 (2021), 5428425.
[66] F. Jiang, et al., A hypoxia gene-based signature to predict the survival and affect the tumor immune microenvironment of osteosarcoma in children, J Immunol Res 2021 (2021), 5523832.
[67] X. Wang, et al., Classification of osteosarcoma based on immunogenomic profiling, Front. Cell Dev. Biol. 9 (2021), 696878.